UCRL 3875

UNIVERSITY OF CALIFORNIA

Radiation Laboratory

BERKELEY, CALIFORNIA

UCRL-3875

UNIVERSITY OF CALIFORNIA

Radiation Laboratory
Berkeley, California

Contract No. W-7405-eng-48

EXPERIMENTS ON ANTIPROTONS: CROSS SECTIONS OF COMPLEX NUCLEI

Lewis E. Agnew, Jr., Owen Chamberlain, Donald V. Keller, Ronald Mermod, Ernest H. Rogers, Herbert M. Steiner, and Clyde Wiegand

July 22, 1957

Printed for the U. S. Atomic Energy Commission

EXPERIMENTS ON ANTIPROTONS: CROSS SECTIONS OF COMPLEX NUCLEI

Lewis E. Agnew, Jr., Owen Chamberlain, Donald V. Keller, Ronald Mermod, Ernest H. Rogers, Herbert M. Steiner, and Clyde Wiegand

Radiation Laboratory
University of California
Berkeley, California

July 22, 1957

ABSTRACT

Experiments are described that have been designed to measure separately annihilation and reaction cross sections for antiprotons of approximately 450 Mev on oxygen, copper, silver, and lead. A new and more luminous spectrograph has been built for this experiment. The antiproton cross sections are compared with total proton cross sections, and are found to be larger by a factor varying from 1.74 for oxygen to 1.39 for silver. Calculations based on the optical model give a reasonable connection between these cross sections and the $\bar{p}$-p and $\bar{p}$-n cross sections. Finally, the information available on antiproton production cross sections is collected. There are indications that a free nucleon is several times as effective as a bound one for producing antiprotons.

EXPERIMENTS ON ANTIPROTONS: CROSS SECTIONS OF COMPLEX NUCLEI*†

Lewis E. Agnew, Jr., Owen Chamberlain, Donald V. Keller, Ronald Mermod, Ernest H. Rogers, Herbert M. Steiner, and Clyde Wiegand

Radiation Laboratory
University of California
Berkeley, California

July 22, 1957

I. Introduction

Immediately following the discovery of the antiproton,[1] experiments were begun to study the properties of the new particle which were not immediately predictable on the basis of Dirac's theory. The first step in this direction was a study of the interaction of antiprotons with complex nuclei.[2] The attenuation of antiprotons in two elements, copper and beryllium, was studied. This first experiment showed two striking features of the interaction of high-energy antiprotons with complex nuclei: an attenuation cross section that was approximately twice as large as that for positive protons, and a large probability for annihilation. Several

---

*This work was done under the auspices of the U. S. Atomic Energy Commission.

†Preliminary reports on this work have been given:
E. Segrè, Bull. Am. Phys. Soc. 2, 36 (1957);
Ypsilantis, Keller, Mermod, Segrè, Steiner, Wiegand, and Chamberlain, Bull. Am. Phys. Soc. 2, 193 (1957);
Owen Chamberlain, in Proceedings of the Seventh Annual Rochester Conference on High-Energy Physics (Interscience, New York, in press).

[1]Chamberlain, Segrè, Wiegand, and Ypsilantis, Phys. Rev. 100, 947 (1955).

[2]Chamberlain, Keller, Segrè, Steiner, Wiegand, and Ypsilantis, Phys. Rev. 102, 1637 (1956).

other experiments involving both counters and photographic emulsions have subsequently been performed;[3,4] all have indicated general agreement with these first results.

It is clear that the original study had to be extended in many directions. For instance, it is desirable to have information concerning the dependence of the cross section on mass number of the target and on the energy of the antiprotons. The distinction between annihilation and scattering cross section had to be made, and the angular distribution of the scattered antiprotons determined. This program involves very complex and lengthy investigations.[5] In this paper we report the results obtained thus far with complex nuclei. The study of hydrogen and deuterium will be reported later. We have up to now used only antiprotons of one energy, about 450 Mev. Our present measurements give separately the annihilation cross sections and attenuation cross sections with cutoff angles of 14.3° and 20.5°. Estimates are also made of the total reaction cross sections.

From the experimental point of view, the first step necessary to conduct this investigation was to improve the antiproton beam. We describe in Section II the new spectrograph used to this end. In Section III we give a description of the attenuation and annihilation experiments and of their evaluation. In Section IV we give whatever information it has been possible to collect up to now on production cross sections of antiprotons. Section V contains a discussion of the experiment and conclusions.

---

[3]Brabant, Cork, Horowitz, Moyer, Murray, Wallace, and Wenzel, Phys. Rev. 102, 498 (1956).

[4]Cork, Lambertson, Piccioni, and Wenzel, Cross Sections of Antiprotons in Hydrogen, Beryllium, Carbon, and Lead. UCRL-3650, Feb. 1957 (to be published in Phys. Rev. 107, July 1, 1957).

[5]Chamberlain, Segrè, Wiegand, and Ypsilantis, Nature 177, 11 (1956).

II. The Spectrograph

The Bevatron beam was accelerated to full energy, 5.8 to 6.3 Bev. The internal beam intensity was from 2×10^{10} to 3×10^{10} protons per pulse, one pulse every 6 seconds. The production targets used were C or $(CH_2)_n$. The internal proton beam was monitored by means of two auxiliary counters in coincidence aimed at the target from a distance of about 15 feet.

The mass spectrograph, which gave a signal whenever an antiproton passed through it, was very similar in structure to the one used previously, but it contained several improvements that greatly increased the luminosity of the apparatus. Indeed, in our original run we had approximately one antiproton every 15 minutes, whereas here the intensity was increased by a factor of approximately 80. This was accomplished by increasing the aperture of the spectroscope and, also, by accepting a momentum interval of ± 3% instead of only ± 1% as before. This relaxation of the momentum definition made the mass determination less stringent, but once antiprotons had been identified, we could afford this uncertainty.

The spectrograph used in this run is shown schematically in Fig. 1. The characteristics of the principal components of this apparatus are given in Table I. The antiprotons produced in a 6-inch-long carbon or polyethylene target in the Bevatron were bent outwards by the field of the Bevatron. A small magnet D was placed as close as possible to the structure of the Bevatron in order to guide the negatively charged beam into the magnetic channel that determined the momentum of the particles. The current in this magnet was varied until the intensity of the negatively charged particle beam was maximum. Upon emerging from the magnet D, the beam of those particles having a momentum 1.19 Bev/c entered a magnetic quadrupole focusing lens Q1, which focused the particles at the center of a second smaller quadrupole lens L. Between these two quadrupole lenses there was a bending magnet M1, which deflected the antiprotons by an angle of 14°. The lens L served as a field lens to guide particles leaving Q1 onto the entrance aperture of the last lens Q2. At the exit of L there was a counter F1 which, in conjunction with another counter F2, was used to determine the time of flight. In the second half of the magnetic channel the magnet M2 bent the beam by another 18.8°, slightly higher than the figure

Table I

	Characteristics of components of the apparatus
T	Bevatron target (production target for antiprotons).
F1	Fitch-type Cherenkov counter of styrene with 2.5% ethyl bromide added: $\mu_D = 1.54$, $\rho = 0.91$ g cm^{-3}; diameter 3.88 in. by 2.31 in. thick.
F2	Same as F1 except diameter 2.5 in.
C1	Cherenkov counter of Fluorochemical 0-75 ($C_8F_{16}O$); $\mu_D = 1.276$; $\rho = 1.76$ g cm^{-3}; 4 in. square by 1.5 in. thick.
C2	Cherenkov velocity-selecting counter of lucite; $\mu_D = 1.50$; $\rho = 1.18$ g cm^{-3}; diameter 2.37 in. by 4.25 in. thick.
S1	Plastic scintillator counter 4.0 in. in diameter by 0.62 in. thick.
E	Area occupied by apparatus and counters for the various experiments.
D	Deflecting magnet 18 in. long; aperture 12 in. wide by 5 in. high; 3.2° bending.
Q1, Q2	Quadrupole focusing magnets of 8-in. aperture.
M1, M2	Deflecting magnets 60 in. long; aperture 12 in. wide by 7 in. high; 14° bending and 18.8° bending respectively.
L	Quadrupole focusing magnet of 4-in. aperture.
C*	Slotted Cherenkov counter of methyl alcohol.
S2	Plastic scintillator counter 14.75 in. in diameter by 0.25 in. thick.
S3	Plastic scintillator counter 13 in. in diameter by 1.0 in. thick.

mentioned above. The antiprotons reaching the counter F2 had a momentum of 1.175 Bev/c because of losses in the gas along the trajectory and in the counter F1. The final focusing was achieved by a third quadrupole lens Q2. The momentum of the beam at F2 was 1.175 Bev/c, with a spread at half maximum of ± 3%. This corresponds to an antiproton energy of 565 ± 35 Mev. The horizontal and vertical intensity distributions of the beam at F2 are shown in Fig. 2. The horizontal distribution shown in Fig. 2 is considerably narrower than that at Counter F1 because the dispersion of the second half of the spectrograph (after F1) compensates for the dispersion of the first half. Ionization energy losses in the remaining counters of the mass spectrograph reduced the mean energy of the beam to 497 Mev upon leaving S1, the last of these counters. The diameter of the beam at this point, defined by Counter S1, was 4 inches, and the beam had a root-mean-square angular divergence of 3^{o}, owing mainly to multiple scattering in F2, C1, and C2.

The scintillator S1 can be considered as the source of our certified antiprotons, which were identified by simultaneous measurement of their momentum and velocity.

The velocity was determined by the use of Counters F1, F2, C1, C2, and S1. F1 and F2 were velocity-selecting Cherenkov counters that discriminated against pions but were sensitive to antiprotons. These counters consisted of liquid styrene radiators (index of refraction 1.543) viewed by one RCA-6810 photomultiplier tube. They detected charged particles in the velocity range $0.65 < \beta < 0.86$. Particles with a velocity below this range did not emit Cherenkov light in the styrene, and the Cherenkov light from particles faster than $\beta = 0.86$ was totally internally reflected and hence not admitted to the photomultiplier tube. The design of these counters is due to Fitch.[6] However, about 10% of the particles with a velocity greater than $\beta = 0.86$ were detected by these counters because they produced fast secondaries in the liquid. Hence, F1 and F2 had a rejection efficiency of only about 90%. Counter C1 consisted of a fluorochemical radiator ($C_8F_{16}O$, designated as 0-75 by the Minnesota Mining

---

[6] V. L. Fitch, Bull. Am. Phys. Soc. Ser. II, 1, No. 1, 52 (1956); invited paper.

and Manufacturing Company) with an index of refraction of 1.276; it counted only charged particles with $\beta > 0.78$ and hence did not detect antiprotons, but did detect the π mesons.

C2 was a special counter that detected particles in the very narrow velocity range $0.74 \leq \beta \leq 0.77$, with a rejection efficiency for faster particles of 97%.[7] Finally, S1 was an ordinary scintillation counter, 4 inches in diameter, which detected all charged particles passing through it. This counter defined the size and divergence of the antiproton beam incident upon the target. Thus, for detecting antiprotons, Counters F1, F2, C2, and S1 were connected in coincidence with one another and C1 was connected in anticoincidence. In conjunction with the attenuation measurements described below, the pulses from various counters following S1 were photographed from an oscilloscope screen, and on the same film the pulses from Counters F1, F2, C1, and S1 were displayed to keep a continuous check on the mass spectrograph.

As a means of checking our results, we also used the spectrograph to select positive protons. For this purpose it was necessary to change the Bevatron-target position slightly, reverse the currents in all magnets of the spectrograph, and then adjust the current in magnet D so that the protons were properly centered on Counter F2. For these runs the Bevatron internal beam was accelerated only to 1.1 Bev. At this energy mesons of 1.175 Bev/c momentum could not be produced.

---

[7] O. Chamberlain and C. Wiegand, The Velocity-Selecting Cherenkov Counter, in Proceedings of the CERN Symposium on High Energy Accelerators and Pion Physics, Vol. 2 (CERN, Geneva, 1956) p. 82.

III. Attenuation and Annihilation in Complex Nuclei

The experimental arrangement used to determine the attenuation and annihilation cross sections is shown in Fig. 3. The material whose cross sections were to be measured was placed in the absorber slots within the Counter C*. Counters S2 and S3 served to determine whether or not a given antiproton (indicated by the selecting apparatus described in the previous section) passed through the absorber (attenuator) and the material of Counter C*. Special attention was given to annihilation events in the attenuator, which could frequently give rise to charged particles that traversed S2 or S3. These annihilation events were separately detected in Counter C*, which was a Cherenkov counter containing methyl alcohol (index of refraction 1.33).

Nuclear-emulsion studies of annihilations of antiprotons[3] have shown that nearly all annihilations give rise to fast charged pions (fast enough to give detectable light in methyl alcohol) or neutral pions (whose γ rays frequently are converted within Counter C* and give detectable Cherenkov radiation). Thus, Counter C* was a very efficient detector of annihilations (efficiency > 90%).

The attenuation materials chosen were copper, silver, and lead. The thicknesses of the absorbers and the average energy of antiprotons or protons at the centers of the attenuators are given below.

Because our antiproton beam had considerable divergence (about 3°) and because the last counter of the mass spectrograph (S1) was rather large (4 in. in diameter), it was not possible to do the attenuation experiment in very "good" geometry. We chose cutoff angles, as shown in Fig. 3, of 14.3° and 20.5°, angles well outside the region of strong diffraction scattering for either antiprotons or protons. This choice was intended to minimize errors due to small changes in geometry of the system. There was some attenuation and annihilation in the methyl alcohol and stainless steel walls of Counter C* so that it was essential to make some runs without any absorbers in the slots of Counter C*. With slots empty, 71% of the antiprotons passed through unaffected--or at most scattered to angles less than 14.3°. When the attenuators were in place in the slots, the corresponding transmissions varied from 32% to 44%, depending on the material used.

Each antiproton indicated by the mass spectrograph was considered an annihilation if it was accompanied by a pulse in the C^* counter, irrespective of whether counts were registered by S2 or S3. If no pulse was seen in the C^* counter, then the presence or absence of pulses in S2 and S3 indicated whether the antiproton in question passed through without scattering (actually , scattered to an angle smaller than 14.3°), or scattered to an angle between 14.3° and 20.5°, or scattered to an angle greater than 20.5°. A scattering process involving scattering by an angle smaller than 14.3° is not detected by this apparatus, hence the quoted cross section results do not include diffraction scattering, which is predominantly to smaller angles.

Although the various annihilation and attenuation data were recorded electronically during the run, there was serious question at the beginning of the run as to how the amplifier gain settings should be made in the signal channel of the C^* counter. The uncertainty was aggravated by the fact that some small scintillation pulses were observed when slow protons (definitely too slow to produce Cherenkov radiation) were passed through the C^* counter. It was therefore necessary to photograph the pulses from the C^* counter, and at the same time the pulses from almost all the other counters were photographed. After the film had been developed and scanned, it was then possible to construct detailed pulse-height curves (or bias curves) for the C^* counter. This, in effect, allowed adjustment of the bias of the counter after the run was finished, and permitted a detailed analysis of annihilation events that gave small pulses in the C^* counter. The photographic recording has unfortunately been very laborious, involving many man-months of film-scanning effort. Each event has been recorded in detail on an IBM card, and an IBM 650 machine has been used to make various types of summations and summaries of the data. When positive-proton cross sections were measured, it was not necessary to use the photographic method because there were no C^* pulses to be analyzed (no annihilations). However, a check of these measurements for protons was also made by the photographic method and it was found that the results agreed with those from the purely electronic detection. It was necessary to construct a reliable extrapolation procedure in order to decide which pulses were due to annihilation and which not. Unfortunately there is no

obvious pulse height for which one can say that all pulses larger than this value, and no others, represent annihilations. Indeed, such a sharp distinction is not to be expected, not only because emulsion data have indicated that the amounts of light to be expected from different stars vary within wide limits, but also because the amounts of light resulting from the same kind of annihilation occurring in different positions in the absorber or C^* counter are different. For instance, annihilations near the end of the C^* counter, where the path length for the resulting charged mesons is short, give little Cherenkov light. Thus we conclude that a few annihilations give small pulses or no pulse in Counter C^*.

On the other hand one may ask if small pulses can be produced by antiprotons that merely pass through C^* without undergoing any nuclear interaction. This is best answered by studying the pulse-height distribution of C^* pulses when positive protons are incident. Even when the momentum of the protons was lower than 1.059 Bev/c, well below the limit at which they could produce Cherenkov light, it was found that there were a few small pulses in Counter C^*, presumably due to some scintillation in the alcohol. We may conclude that only some of the small pulses in C^* represent annihilations, and that some annihilations are included in the events for which no pulse in C^* occurs. In order to resolve this dilemma we used the following procedure: We plotted in histograms the numbers of events with the C^* pulse greater than a given value. As an example, such plots are shown in Figs. 4 and 5. The points on the solid curve represent an integral of the pulse-height histogram starting from the right. The integral curve shows a reasonable plateau if we omit the very small pulses that are almost certainly due to causes different from antiproton annihilation. We can then extrapolate from the flat part of the plateau and obtain an extrapolated number of pulses. Similar diagrams were obtained for various values of the photomultiplier voltage on the C^* counter, and it was verified that the results of the extrapolation agreed among themselves regardless of the voltage. Using procedures of this type, we determined the numbers of events in each of the following categories:

a. I_0 = the number of incident particles (antiprotons or protons) on the attenuator = the total number of acceptable events.

b. I_{an} = the number of annihilation events.

c. $I(20^\circ)$ = the number of pass-through particles with a cutoff angle $\theta_c \leq 20^\circ$. This equals the number of nonannihilation events that count in S2.

d. $I(14^\circ)$ = the number of pass-through particles with a cutoff angle $\theta_c \leq 14^\circ$. This equals the number of nonannihilation events that count in S3.

e. $I_{an}(< 20^\circ)$ = the number of annihilation events in which charged particles count in S2.

f. $I_{an}(< 14^\circ)$ = the number of annihilation events in which charged particles count in S3.

g. $I_{an}(> 20^\circ)$ = the number of annihilation events in which no charged particle counts in S2.

h. $I_{an}(> 14^\circ)$ = the number of annihilation events in which no charged particle counts in S3.

We have the following obvious relations:

i. $I_{an} = I_{an}(< 20^\circ) + I_{an}(> 20^\circ) = I_{an}(< 14^\circ) + I_{an}(> 14^\circ)$.

j. $I_{an}(< 20^\circ) + I(20^\circ)$ = total number of counts in S2.

k. $I_{an}(< 14^\circ) + I(14^\circ)$ = total number of counts in S3.

The formula for the attenuation cross sections $\sigma(\theta_c)$ at cutoff angle θ_c is

$$\sigma(\theta_c) = \frac{1}{N} \ell n \left(\frac{I_0}{I(\theta_c)} \quad \frac{I'(\theta_c)}{I'_0} \right),$$

where the I are as defined previously, and the I' have the same meaning as the corresponding I but are measured without any absorber in the slots; they are background data. N is the thickness of the absorber in the slots in nuclei per square centimeter. Table II gives the data relative to the absorbers.

Table II.

Characteristics of attenuators

Material	Thickness ($g\ cm^{-2}$)	Thickness ($atoms\ cm^{-2}$)	Average beam kinetic energy at center (Mev)
Cu	67	0.644×10^{24}	411
Ag	53	0.296×10^{24}	431
Pb	58	0.1678×10^{24}	436

As an example to indicate how the cross sections were determined from the original data, we describe here in detail the calculation of the cross sections for antiprotons on copper. The data are shown in Table III.

Table III

Data obtained for antiprotons incident on a copper attenuator. The copper thickness is indicated in Table II. Data are also given for the case in which the slots are empty (background data, indicated in the text as I_0', $I'(14^\circ)$, etc.).

Quantity evaluated	Number of events, copper in slots	Number of events slots empty
I_0	1951	1100
$I(14^\circ)$	628	785
$I(20^\circ)$	651	805
I_{an}	1180	250
$I_{an}(< 14^\circ)$	205	65
$I_{an}(< 20^\circ)$	332	95

To give some idea what was involved in the extrapolation procedure used to correct for imperfections in the counter C^*, we may comment that for $I(14^\circ)$ the extrapolation changed the raw number 647 to 628 (shown in Table III). The background extrapolation accounted for a change of about the same magnitude.

Because the elastic diffraction cross section is almost all contained within angles smaller than 14°, it is possible to estimate the total reaction cross section by extrapolating to zero solid angle subtended by the counter (meaning Counter S_2 or S_3). The method is the same as that used by Chen, Leavitt, and Shapiro,[8] and is not described further in this paper. Since the extrapolations add very little to the cross sections, the method should be quite adequate for our needs. The computed reaction cross sections are listed with the results.

[8] Chen, Leavitt, and Shapiro, Phys. Rev. 99, 857 (1955); see especially Fig. 5 of that paper.

The statistical errors in the determination of the cross sections are given by the formula

$$\Delta\sigma(\theta_c) = \frac{1}{N}\left[\frac{1}{I(\theta_c)} - \frac{1}{I_0}\right]^{1/2}.$$

To this we must add the error due to the extrapolation of the data mentioned previously. This has been estimated and $\Delta\sigma$ has been increased by a factor of about 1.4 in order to take the last error into account. The results are given in Table IV. In this table we have also included for comparison the cross sections obtained with a proton beam. These agree reasonably well with data obtained elsewhere. The data of Table IV agree also with the data previously obtained by us.

Table IV

Antiproton and proton cross sections in millibarns. T is the kinetic energy at the center of the attenuator. $\sigma(14^{o})$ is the cross section for annihilation and nuclear absorption plus the cross section for scattering to angles larger than 14^{o}. $\sigma(20^{o})$ is similarly defined. σ_{an} is the annihilation cross section. σ_{r} is the total reaction cross section (see text for extrapolation procedure). $\bar{p}$ indicates antiprotons, and p^{+} indicatates protons.

Element	T (Mev)	$\sigma(14^{o})$ $\bar{p}$	$\sigma(14^{o})$ p^{+}	$\sigma(20^{o})$ $\bar{p}$	$\sigma(20^{o})$ p^{+}	σ_{an} $\bar{p}$	σ_{r} $\bar{p}$	σ_{r} p^{+}	$\frac{\sigma_{r}\bar{p}}{\sigma_{r}p^{+}}$	$\frac{\sigma_{r}\bar{p}}{\sigma_{an}}$
O[a]	457	556±10	292±2	517±10	246±2	453±9	590±12	340±4	1.74±0.04	1.36±0.04
Cu	411	1240±82	719±5	1220±88	640±4	1040±61	1260±91	880±10	1.44±0.11	1.19±0.10
Ag	431	1630±170	1052±6	1640±183	924±6	1500±157	1635±188	1170±12	1.39±0.16	1.09±0.17
Pb	436	2910±222	1722±20	2680±254	1461±10	2010±182	3005±275	1845±40	1.62±0.16	1.49±0.20
		2850±225[b]	1662±36[b]							

[a] Oxygen cross sections are based upon data to be described in a later paper. The data in question were obtained in connection with a H_2O-O_2 subtraction experiment to determine the hydrogen (and deuterium) cross sections.

[b] Corrected for multiple scattering effects as calculated using the results of Sternheimer, Rev. Sci. Instr. 25, 1070 (1954). Similar corrections for O, Cu, and Ag were not significant.

IV. Production Cross Sections for Antiprotons

In the course of these experiments it has been possible to estimate absolute differential antiproton production cross sections, and, by using alternatively two different targets in the Bevatron, to compare the differential production cross sections for two elements, hydrogen and carbon. The cross sections refer to production at 0^{o} in the forward direction and are per unit solid angle and unit momentum interval of the antiproton. We do not know whether the antiprotons are formed by a $p + p \rightarrow 3p + \bar{p}$ reaction or by a two-step reaction involving the formation of pions as a first step.[9]

Our mass spectrograph includes two momentum analyzers--one composed of the magnets before Counter F1, the other the magnets following F1. It is not trivial to estimate the transmission of this whole system, because it is difficult to determine what fraction of the particles transmitted by the first analyzer succeed in passing through the second analyzer. It is possible, however, to make a reliable estimate of the effective solid angle and effective momentum interval of the first momentum analyzer. One can then determine, once the beam intensity is known, the differential cross section (cross section per unit solid angle and unit momentum interval) for production of charged particles at the target. The second momentum analyzer and associated counters can then be used to determine what fraction of the charged particles consists of antiprotons. Although the counter arrangement used in the work reported here was not such as to allow an accurate count of the total numbers of charged particles reaching F1 (because F1 was not sensitive to all charged particles), we have used this method and the data of an earlier run to determine the differential cross section for antiproton production from a copper target. The result is 1.1×10^{-30} cm^2 $sterad^{-1}$ $(Bev/c)^{-1}$ for the production differential cross section per nucleon in copper for antiprotons of momentum 1.19 Bev/c emerging in the forward direction from a copper target bombarded by 6.1-Bev

---

[9] G. Feldman, Phys. Rev. 95, 1967 (1954).

protons.[10] This result is uncertain by a factor of about 2, mainly because the solid angle of the spectrograph has not been determined precisely and the beam monitoring was somewhat uncertain.

In this run we have made a comparison of the antiproton production in carbon (graphite) with the production in CH_2 (polyethylene), and from this we have deduced the production in hydrogen relative to that in carbon. With available target mechanisms it was impossible to have the two alternately used targets in the same position within the Bevatron; the centers of the two had to be separated by about 1 foot. To determine the effects of this difference in target positions, the two targets were interchanged during the run. Unfortunately it was necessary to admit air to the whole Bevatron vacuum system in order to interchange the targets, hence only one such interchange could be made during the run. The results are therefore somewhat tentative, and it is our expectation that the antiproton production in hydrogen will be remeasured at the earliest opportunity. Our result may be quoted as follows: the ratio of differential cross sections for producing antiprotons by bombarding carbon and by bombarding hydrogen is 0.11 ± 0.06. If this is expressed as the ratio per nucleon, then the production in hydrogen divided by the production in carbon is 1.3 ± 0.7. In each case we are discussing differential production cross sections for antiprotons of momentum 1.19 Bev/c emerging in the forward direction from targets bombarded with 6.1-Bev protons.

The above result is at first sight surprising, in that the statistical theory of antiproton production predicts less production per nucleon in hydrogen than in carbon. This is because the momentum of the nucleons within the carbon nucleus should be important in giving increased production in carbon when the bombarding energy (6.1 Bev) is so close to the threshold energy (5.6 Bev) for producing antiprotons in collisions with hydrogen. Rough statistical calculations of the total antiproton

---

[10] This value supersedes one given previously by E. Segrè, A Review of the Antiproton Work at Berkeley, in Proceedings of the CERN Symposium on High Energy Accelerators and Pion Physics, Vol. 2 (CERN, Geneva, 1956), p. 107 and normalizes the highest point of Fig. 5 of Ref. 1.

production in hydrogen and carbon have indicated that the total production (per nucleon) in hydrogen should be not more than 0.12 of the total production per nucleon in carbon. (Compare with the experimental number 1.3.) We have not made a corresponding calculation of the ratio of differential cross sections according to the statistical theory, but it seems very doubtful that the theory would agree with our result. However, the caluclations have been made without taking into account two effects that could well explain the apparent discrepancy: the reabsorption of antiprotons within the carbon nucleus, which may be expected to be quite appreciable, and the fact that the antiprotons produced by collisions with bound protons acquire a larger transverse momentum and are thus spaced over a larger solid angle.

Discussion

The results given in this paper are for the most part in reasonable agreement with results given earlier, where a comparison can be made. The present measurement of the annihilation cross section for copper, (1040 ± 61) mb, agrees well with the previous result, (1050 ± 220) mb. For lead, the annihilation cross section is in good agreement with the trend of the curve of $\sqrt{\frac{\sigma_n}{\pi}}$ versus $A^{1/3}$ (see below), whereas the total inelastic cross section measurement seems anomalously high. Whether or not this fact can be attributed to inadequate compensation for multiple scattering or some other systematic error will be shown by further experiments. The value of σ_r for lead given here is (3005 ± 254) mb, which is to be compared with the earlier result[4] of (2330 ± 650) mb. Finally, our positive proton cross sections are in agreement, within about 7 mb, with those obtained at Brookhaven[8] with a similar geometry at a somewhat higher energy.

In order to show some of the trends inherent in the present results we refer to Fig. 6. The abscissa is $A^{1/3}$ and the ordinate is $(\sigma_r/\pi)^{1/2}$, which we may call the reaction radius; σ_r is the reaction cross section. A straight line on this plot would then represent the equation

$$\sigma_r = \pi R^2 = \pi(a + r_0 A^{1/3})^2.$$

The experimental values of σ_r are indicated in the figure for antiprotons incident on O, Cu, Ag, and Pb. These points have been fitted by the least-squares method to a straight line. The slope of this line is r_0--the radius parameter. If the point for lead (about which there is some doubt) is omitted, the value of r_0 thus obtained is $1.29 \pm 0.08 \times 10^{-13}$ cm. Similar plots are included for the annihilation cross section for antiprotons and for

the reaction cross sections for ordinary protons. The results for the respective slopes are 1.29 ± 0.08 and $1.31 \pm 0.01 \times 10^{-13}$ cm, where only statistical errors have been included. Following the line of argument suggested by this plot, one may somewhat loosely say that all these processes indicate approximately the same value of the radius constant r_0, but that the different intercepts suggest a large range of interaction for the antiproton.

In order to make this argument a little more quantitative, we shall try to treat the p^--nucleus collision by an optical model.[11] In order to apply this model we need to know the nuclear density in a nucleus. We assume for this

$$\rho(r) = \rho_0 \left(\exp\left(\frac{r-c}{z}\right) + 1\right)^{-1}. \tag{5.1}$$

This form of nuclear density distribution is suggested by electron-scattering experiments,[12] and we use the same constants as Hofstadter,

$$c = 1.08\, A^{1/3} \times 10^{-13} \text{ cm and } z = 0.57 \times 10^{-13} \text{ cm}.$$

The constant ρ_0 is adjusted to the correct total number of nucleons, instead of correct nuclear charge as in Hofstadter's paper.

The formula for the reaction cross section is

$$\sigma_r = 2\pi \int_0^R \left(1-e^{-2Ks}\right) bdb = 2\pi \int_0^R \left(1-e^{-2Ks}\right) sds, \tag{5.2}$$

for a uniform nucleon distribution within a sphere of radius R where $s^2 = R^2 - b^2$, b is the impact parameter with respect to the center of the nucleus, and K is the absorption coefficient given by $K = 3A\bar{\sigma}/4\pi R^3$ with $\bar{\sigma}$ the average total nucleon-nucleon or nucleon-antinucleon cross section. In order to refine this formula, we first want to replace Ks by

$$\bar{\sigma} \int_0^\infty \rho(r)ds,$$

which obviously reduces to Ks in the case of uniform density. However, we must also take into account the finite range of interaction of nucleon and nucleon or nucleon and antinucleon. The effect of a finite range of interaction

---

[11] Fernbach, Serber, and Taylor, Phys. Rev. 75, 1352 (1949).

[12] R. Hofstadter, Revs. Modern Phys. 28, 214 (1956).

is particularly important for incident antinucleons because the elementary cross sections are large. Measurements reported in the following paper give, for an energy of 457 Mev, $\sigma_{\text{total } \bar{p}p} = 104$ mb (to be compared with $\sigma_{\text{total } pp} = 28$ mb), and similar results for $\bar{p}n$ and pn. We take into account the range of interaction by replacing the density ρ by a smeared density $\bar{\rho}$ given by

$$\bar{\rho}(r) = \int F\left(\left|\underset{\sim}{r} - \underset{\sim}{r}'\right|\right) \rho(r')\, d^3\underset{\sim}{r}', \tag{5.3}$$

in which F is a smearing function. We have chosen $F(x) = 3/4\, \pi\, \eta_0^3$ for $x < \eta_0$ and

$$F(x) = 0 \tag{5.4}$$

otherwise. The smeared density at a certain point is thus the average of the actual density over a sphere of radius η_0. Our calculated reaction cross section is then

$$\sigma_r = 2\pi \int_0^\infty bdb \left\{1 - \exp\left[-2\bar{\sigma} \int_0^\infty \bar{\rho}\, ds\right]\right\}, \tag{5.5}$$

where $\bar{\rho}$ is obtained from Eq. (5.3).

Accepting the density distribution of Eq. (5.1), we have two free parameters, namely the smearing radius η_0 and the elementary cross section $\bar{\sigma}$. We take $\bar{\sigma}$ as 104 mb, from experiment. We find η_0 by imposing the requirement that the cross section of a single nucleon (represented by $\rho(r) = \delta(r)$ in Eq. (5.3)) be $\bar{\sigma}$ also.

The calculated results are compared with experiment in Table V and Fig. 7. Besides the experimental values of reaction cross sections and annihilation cross sections we give the reaction cross sections calculated with $\eta_0 = 0$ (no smearing) and with $\eta_0 = 2.0 \times 10^{-13}$ cm (η_0 determined as outlined in the text, above.)

Table V

Experimental and calculated values of the cross sections. The calculated values are for zero range ($\eta_0 = 0$) and for $\eta_0 = 2.0 \times 10^{-13}$ cm and $\bar{\sigma} = 104$ mb. The cross sections are given in millibarns.

	Experimental results		Calculated values	
Element	σ_r	σ_{an}	$\eta_0 = 0$	$\eta_0 = 2 \times 10^{-13}$ cm
Oxygen	590 ± 12	453 ± 9	493	576
Copper	1260 ± 91	1040 ± 61	1029	1181
Silver	1633 ± 188	1500 ± 157	1406	1564
Lead	(3005 ± 250)	2010 ± 182	2012	2209

Comparing the first and last columns of Table V, we see that this model is adequate--at least for the time being.

Similar calculations have been performed by G. Goldhaber[13] and S. Drell.[14]

ACKNOWLEDGMENTS

We wish to express our appreciation to Professors E. Segrè and T. Ypsilantis for consultation during the course of this experiment. In addition the cooperation and help of Dr. Edward J. Lofgren and the staff of the Bevatron was greatly appreciated.

[13] G. Goldhaber, private communications. See Proceedings of the Seventh Annual Rochester Conference on High-Energy Physics, 1957 (Interscience, New York, in press). Antibaryon Session.

[14] S. Drell, private communications. See Proceedings of the Seventh Annual Rochester Conference on High-Energy Physics, 1957 (Interscience, New York, in press). Antibaryon Session.

Figure Legends

Fig. 1. Spectrograph used for the detection of antiprotons. For characteristics of parts see Table I.

Fig. 2. Beam profiles at F_2.

Fig. 3. Arrangement of counters for detecting separately the annihilation and the scattering of antiprotons.

Fig. 4. Pulse-height histogram for 1.175-Bev antiprotons on Cu in the C^* counter, with 2000 volts on C^*. The solid curve is the integral of the histogram from the right, showing the method of extrapolation. In this example, only events for which counter S3 did not count are included.

Fig. 5. Pulse-height histogram for 1.175-Bev antiprotons on Cu in the C^* counter, with 2200 volts on C^*. The solid curve is the integral of the histogram from the right, showing the method of extrapolation. In this example, only events for which counter S3 did not count are included.

Fig. 6. Plot of $\sqrt{\frac{\sigma}{\pi}}$ vs $A^{1/3}$ for the three cross sections $\sigma_r^{\bar{p}}$, $\sigma_{an}^{\bar{p}}$, and $\sigma_r^{p^+}$.

Fig. 7. σ_r versus $A^{1/3}$ for a Fermi density model modified by a square-well interaction of range η.

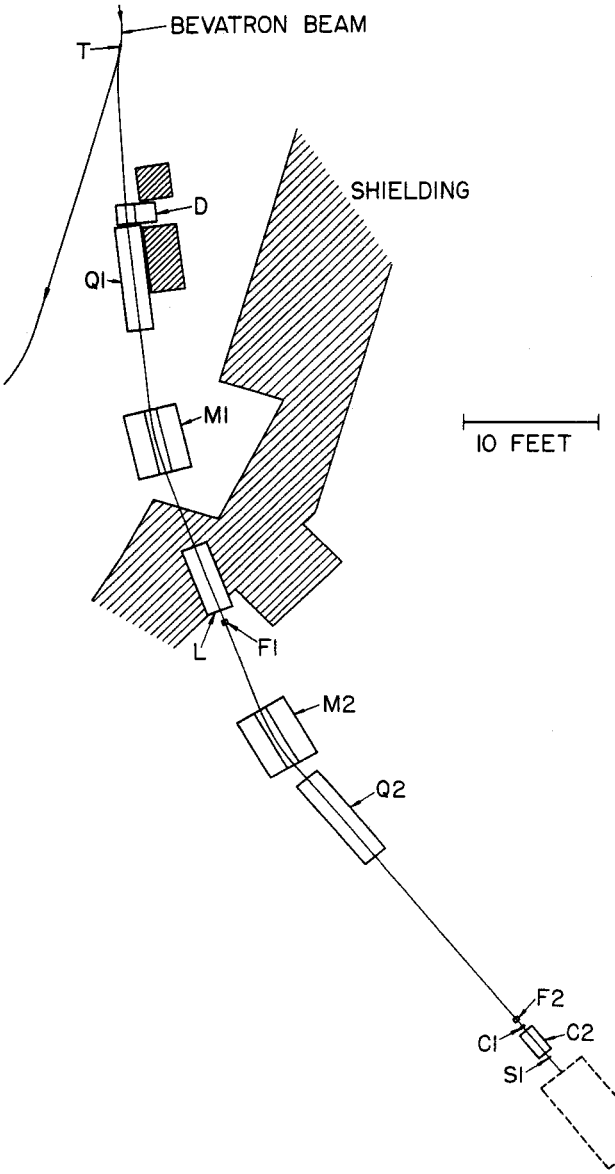

MU-12666

Fig. 1

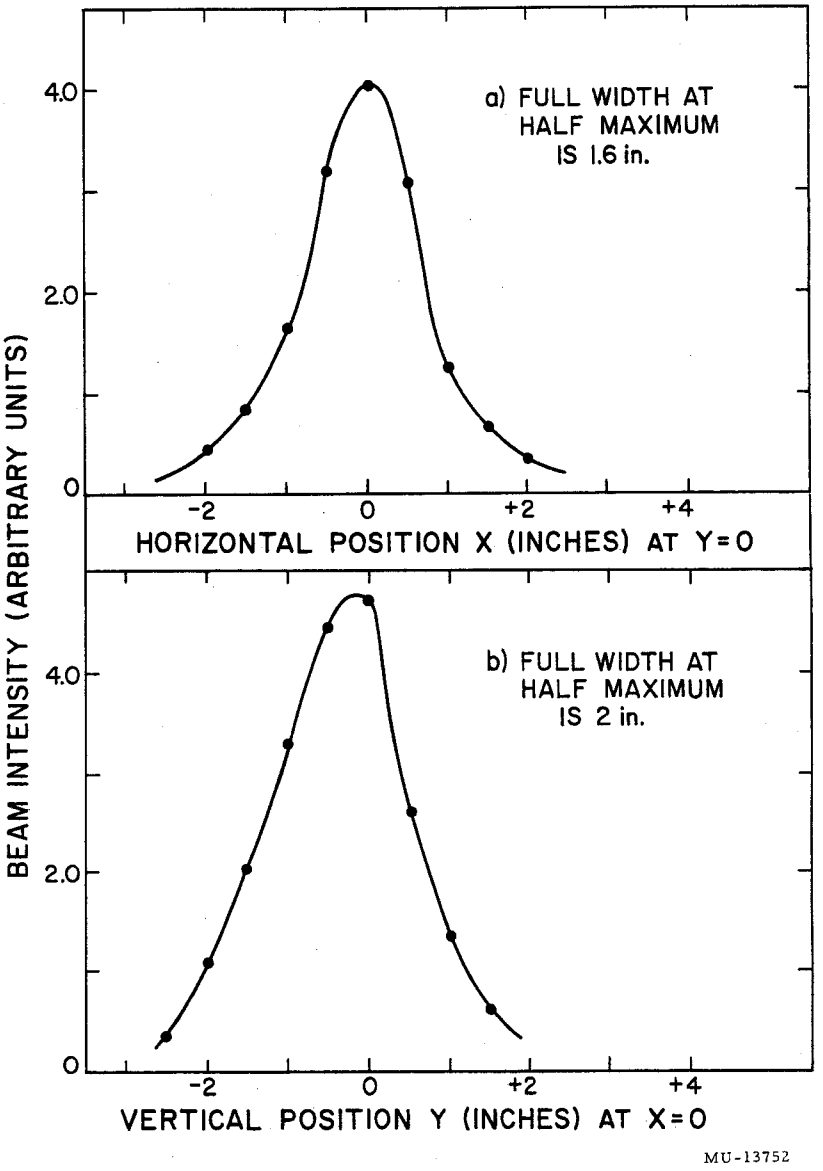
a) FULL WIDTH AT HALF MAXIMUM IS 1.6 in.
b) FULL WIDTH AT HALF MAXIMUM IS 2 in.
BEAM INTENSITY (ARBITRARY UNITS)
4.0
2.0
0
-2
0
+2
+4
HORIZONTAL POSITION X (INCHES) AT Y=0
VERTICAL POSITION Y (INCHES) AT X=0
MU-13752

Fig. 2

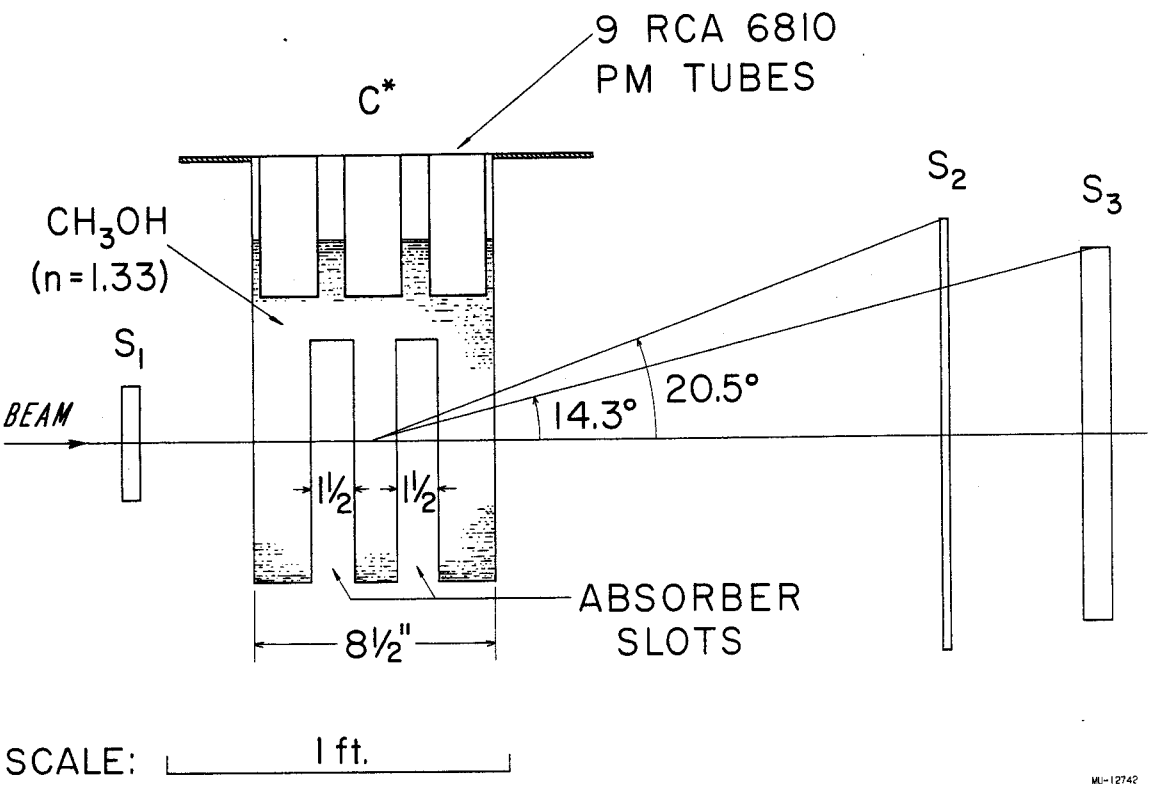
9 RCA 6810
PM TUBES
C*
S_2
S_3
CH_3OH
(n=1.33)
S_1
BEAM
14.3°
20.5°
1½
1½
ABSORBER
SLOTS
8½"
SCALE:
1 ft.
MU-12742

Fig. 3

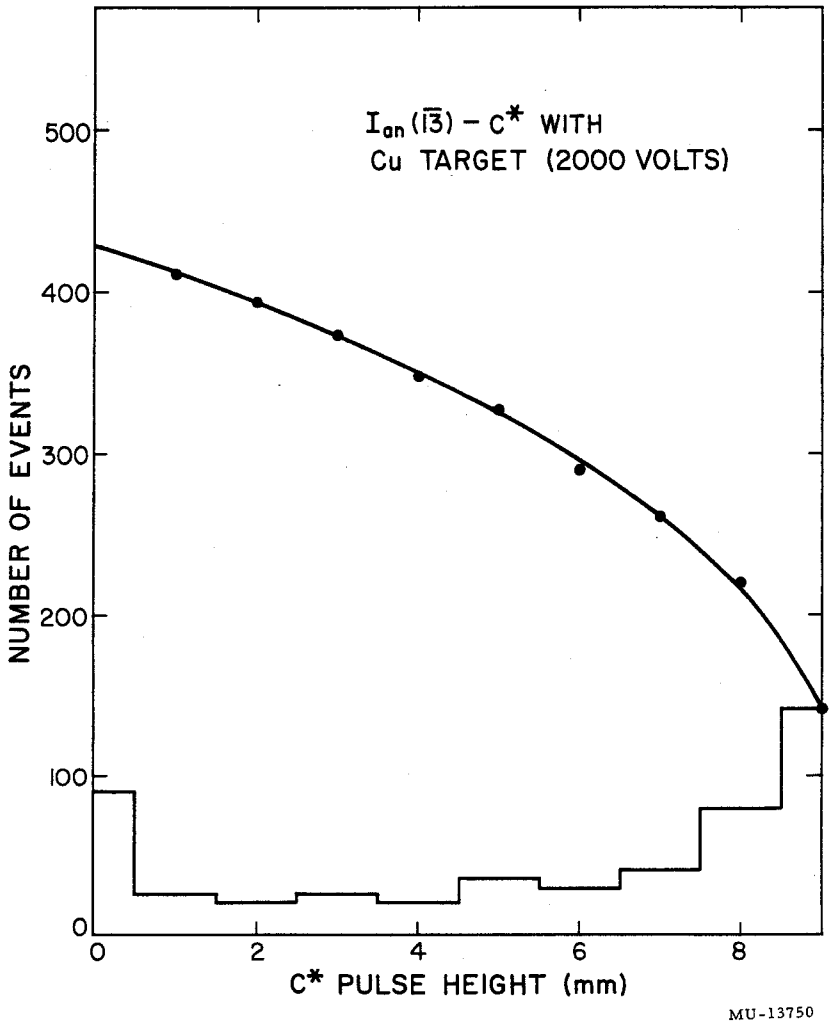
$I_{an}(\bar{1}\bar{3})$ – C* WITH
Cu TARGET (2000 VOLTS)
NUMBER OF EVENTS
500
400
300
200
100
0
0
2
4
6
8
C* PULSE HEIGHT (mm)
MU-13750

Fig. 4

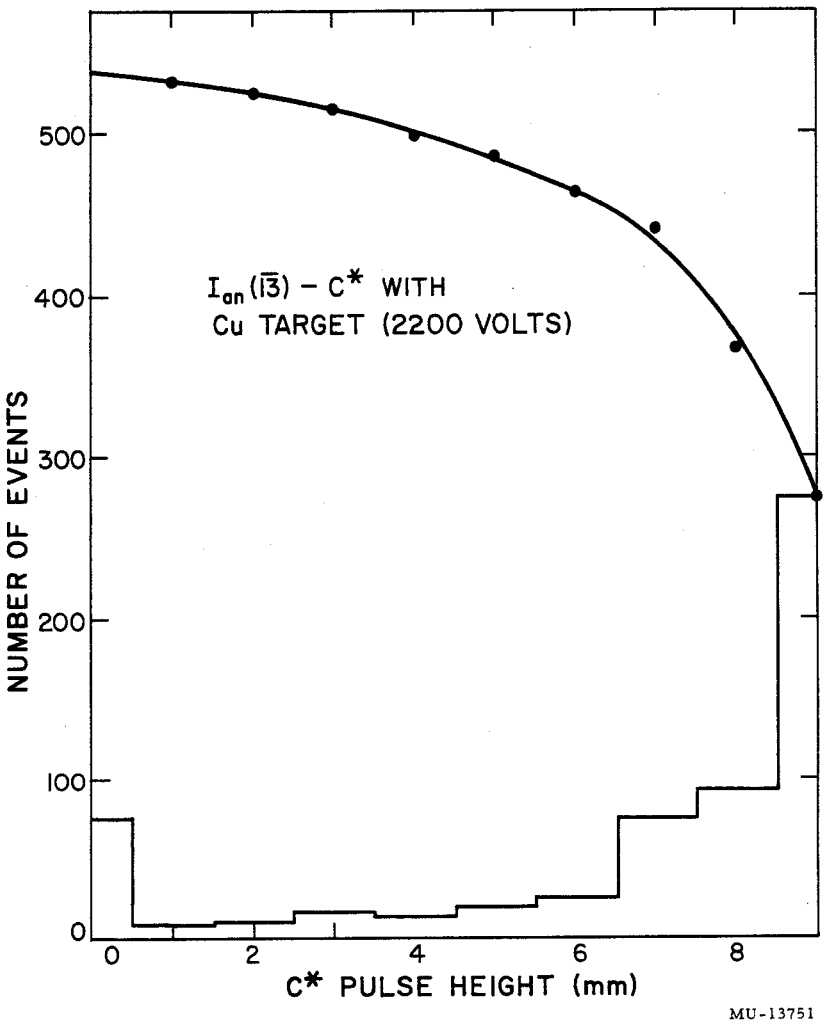
$I_{an}(\bar{1}\bar{3})$ – C* WITH
Cu TARGET (2200 VOLTS)
NUMBER OF EVENTS
500
400
300
200
100
0
0
2
4
6
8
C* PULSE HEIGHT (mm)
MU-13751

Fig. 5

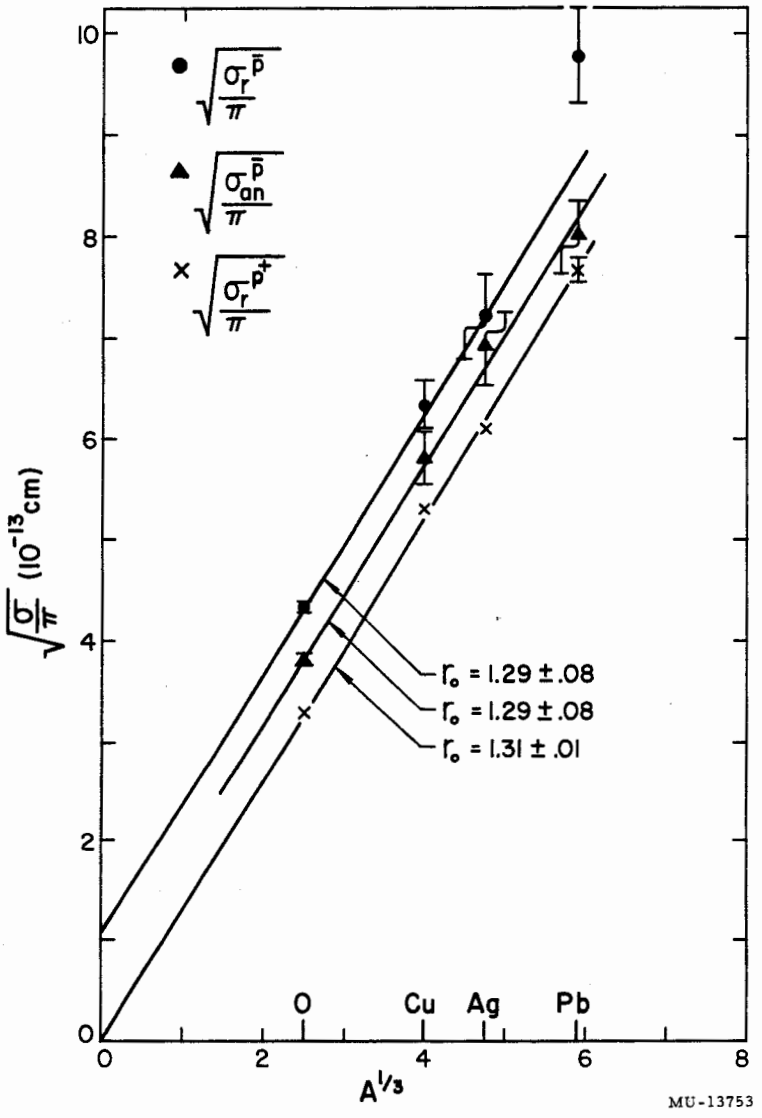
$\sqrt{\frac{\sigma_r^{\bar{p}}}{\pi}}$
$\sqrt{\frac{\sigma_{an}^{\bar{p}}}{\pi}}$
$\sqrt{\frac{\sigma_r^{p^+}}{\pi}}$
$\sqrt{\frac{\sigma}{\pi}}$ (10^{-13} cm)
$r_o = 1.29 \pm .08$
$r_o = 1.29 \pm .08$
$r_o = 1.31 \pm .01$
O
Cu
Ag
Pb
$A^{1/3}$
MU-13753

Fig. 6

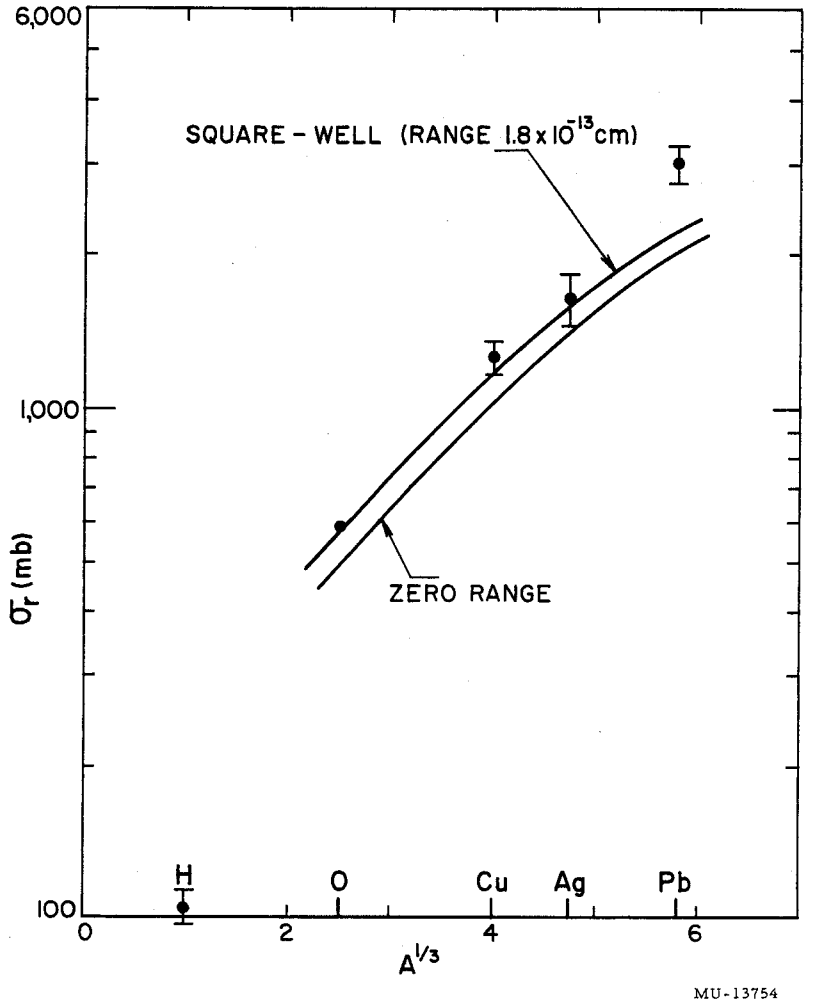
6,000
1,000
100
SQUARE - WELL (RANGE 1.8 x 10⁻¹³ cm)
ZERO RANGE
σr (mb)
H
O
Cu
Ag
Pb
0
2
4
6
A^1/3
MU-13754

Fig. 7